



# Nano Science and Nano Technology

*An Indian Journal*

*Full Paper*

NSNTAJ, 9(2), 2015 [064-074]

## Water detoxification using gamma and alfa alumina nanoparticles prepared by micro emulsion route

M.A.Ahmed<sup>1</sup>, Samiha T.Bishay<sup>2\*</sup>, Rania Ramadan<sup>1</sup>

<sup>1</sup>Materials Science Lab (1), Physics Department, Faculty of Science, Cairo University, Giza, (EGYPT)

<sup>2</sup>Physics Department, Faculty of Girls for Arts, Science and Education, Ain Shams University, Cairo, (EGYPT)

E-mail: dr\_samiha@hotmail.com

### ABSTRACT

Reverse micro emulsion route with subsequent several heat-treatments was considered to synthesize  $\gamma$  and  $\alpha$  alumina nanoparticles. The study clarified that metastable  $\gamma$ -Al<sub>2</sub>O<sub>3</sub> phase was gross through the annealing temperature (650°C-900°C) with particle size ranged (2nm-4nm). The increase of temperature to more than 900°C, leads to a well formation of stable  $\alpha$ -Al<sub>2</sub>O<sub>3</sub> with particle size 80nm. The investigations confirmed that,  $\gamma$ -alumina is characterized by its great roughness, surface area and pore volume, while  $\alpha$ -alumina is distinct by small porosity. These two alumina phases were tested in water detoxification. Their efficiency to remove lead from water was measured. The measurements indicated that the removal efficiency after 7h for  $\gamma$  and  $\alpha$  alumina reaches 94.5% and 92% respectively. These results together with the characteristic study of roughness and porosity recommended that  $\gamma$ -Al<sub>2</sub>O<sub>3</sub> can be applied as catalyst support in adsorption of toxic heavy metals, while,  $\alpha$ -Al<sub>2</sub>O<sub>3</sub> can be used in fabrication of water desalination membrane.

© 2015 Trade Science Inc. - INDIA

### KEYWORDS

Alumina;  
Nanostructures;  
Chemical synthesis;  
Adsorption of toxic heavy metals.

### INTRODUCTION

The heavy metals are introduced into natural water resources by waste water discharged from industries such as smelting, metal plating, cadmium, nickel and lead storage batteries, phosphate fertilizer, mining, galvanizing, paints, pigments, cosmetics, stabilizer and alloy manufacturing<sup>[1-4]</sup>. The removal of heavy metals from natural waters or soils is very critical. It represents an essential topic that has attracted a considerable attention. It could enter the food chain through drinking water and crop irri-

gation from waste water which is considered to be a widespread problem. Lead is nonbiodegradable and tends to bio-accumulate in cells of the living organisms<sup>[5]</sup>. Lead causes severe damage to the kidney, nervous and reproductive systems, liver and brain. The conventional technologies for the removal of heavy metal ions from aqueous solution include chemical precipitation, ion exchange, reverse osmosis, electrochemical treatment and adsorption<sup>[6-12]</sup>. Among the different treatments described above, adsorption technology is attractive due to its merits of efficiency, economy and simple operation method

without yielding harmful by-products<sup>[13]</sup>.

Now, most of researchers directed to alumina studies have considered the adsorption of toxic material such as  $Pb^{2+}$ ,  $Cd^{2+}$ ,  $Zn^{2+}$  and  $Ni^{2+}$ <sup>[14,15]</sup>. Alumina nanoparticle with different phases is the most preferable method to remove heavy metals. Physical phenomena related to the growth and phase formation of alumina,  $Al_2O_3$ , were investigated<sup>[16-23]</sup>. The usual synthesis of the transition alumina phase consists of two steps. The first step is the preparation of alumina hydrates such as amorphous aluminum hydroxide, bayerite, and boehmite. The second is the transformation from alumina hydrates to alumina through thermal decomposition by calcination. The metastable phase ( $\gamma$ ) is involved in transition sequences, which all irreversibly end in the transformation to the stable ( $\alpha$ ) phase at high degree of temperature depending on the preparation techniques. Thus, achieving low-temperature growth of  $\alpha$ -alumina and/or high-temperature stability of metastable alumina are the main goals of the present study, which would be of great importance and would increase the range of possible applications<sup>[24]</sup>. Several researchers<sup>[25-27]</sup> studied the different phases of alumina to choose the most important one in applications in catalysis<sup>[28-32]</sup>, optics<sup>[33]</sup>, electronics<sup>[34]</sup>, adsorption<sup>[35]</sup> and biomedical applications<sup>[36]</sup>.

Numerous methods have been adopted for synthesis  $Al_2O_3$  nanoparticles, which include mechanical milling, sol-gel method<sup>[37-40]</sup>, hydrolysis and precipitation, hydrothermal method, combustion synthesis, and electrospinning method<sup>[21,41]</sup>. Water-in-oil (W/O) microemulsions or reverse microemulsions technique is one of the most recognized methods<sup>[18]</sup> due to its advantages, such as, soft chemistry, demanding no extreme pressure or temperature control, easy handling, and requiring no special or expensive equipment, and was invented as an effective process for preparing nanoparticles<sup>[42]</sup>. W/O microemulsion is coexistence of excess water phase and the surfactant molecules that aggregate in the oil phase in the form of reverse micelle<sup>[18]</sup>.

In the present work, alumina nanoparticles were prepared using reverse microemulsion method. The morphology, particle size and composition were studied as a function of the heat treatment for the

prepared samples. The synthesized  $\gamma$ - $Al_2O_3$  and  $\alpha$ - $Al_2O_3$  nanoparticles were employed as a sorbent for removal of lead metal from water. The effects of pH and the contact time on the adsorption process were studied and optimized.

## EXPERIMENTAL

### Sample preparation

All the chemicals used here to synthesis  $Al_2O_3$  were of analytical grade, aluminum nitrate ( $Al_2(NO_3)_3 \cdot 9H_2O$ ), ammonia ( $NH_3 \cdot H_2O$ ), Triton X-100 (polyethylene glycol octylphenyl ether), n-butyl alcohol, cyclohexane, nitric acid and lead nitrate.

Cyclohexane, Triton (X-100) and butanol were used as oil phase, surfactant and co-surfactant mixed magnetically with a magnetic stirrer (MODEL 78-1) with ratios 20:1:4 until the mixture becomes transparent. The mixture was divided into two parts. 1.6 M  $Al_2(NO_3)_3$  was added to the first part while ammonia was added to the second part until pH equals 11. Then the mixture containing ammonia was added drop by drop to the mixture containing  $Al_2(NO_3)_3$  until pH is adjusted at 8.5-9. The final mixture was stirred using magnetic stirrer for one hour and then aging for 24 h. The precipitate washed with ethanol by ultrasonic (Wise clean) and followed by centrifugation. The powder was dried for an hour at 60°C. Then the powder was annealed for two hours at different temperature 650-1150°C.

### Sample characterization

X-ray diffraction analyses were carried out using a Proker D<sub>8</sub> advance X-ray diffractometer with  $CuK_{\alpha}$  radiation ( $\lambda = 1.5418 \text{ \AA}$ ) to identify phases formation of  $Al_2O_3$  after each calcination temperature. The X-ray diffraction pattern was recorded at room temperature in a wide range of Bragg angles  $2\theta$  ( $20^\circ \leq 2\theta \leq 80^\circ$ ) with  $0.02^\circ$  step size. The crystallite size was calculated from the X-ray data using Scherrer's formula<sup>[43]</sup>. FTIR spectra were obtained with JASCO-FTIR-4100 using the potassium bromide; each spectrum was collected after 32 scans between 400 and 4000  $cm^{-1}$  at a resolution of 4  $cm^{-1}$ . Scanning electron micrographs as well as energy

## Full Paper

dispersive X-ray analysis (EDX) of the investigated samples were performed using SEM (JEOL-JSM 6100), operating at 30kV as an accelerating voltage. EDX was used to examine the morphology of the surface and percentage of Al and O. AFM of model Wet – (SPM-9600) (Scanning Probe microscope, Shimadzu made in Japan Non-Contact mode) has been used to measure the roughness, porosity and surface area of the investigated samples. AFM was performed to measure the vertical and horizontal deflection of the cantilever with pico-meter resolution. Zeta potential measurements of the two phases of alumina nanoparticles dispersed in water have been obtained using zeta seizer nano series (Nano ZS), Malvern, UK, size range 0.6 to 6000 nm and zeta potential range of (-200 to 200 mV). The concentrations of heavy metal ions after reacting with alumina have been analyzed at different pH and time with an atomic absorption spectrometer (PERKIN ELMER A. Analyst 100) using standard atomic solution.

### Batch experiment of Pb<sup>2+</sup> removal

To study the optimum pH values of Pb<sup>2+</sup> adsorption, the experiments were carried out in a series of 250 mL flasks containing (0.1 g/L) of nano alumina powder in 2ppm of lead nitrate. Lead ions adjusted at different pH values from 2-11. The investigated solutions were dispersed well using electric shaker (ORBITAL SHAKER SO1) at 250 rpm for 60 min at room temperature. The supernatant solutions were then collected and filtered through 0.2µm syringe filter. Lead concentrations in the filtrate were measured using atomic absorption spectroscopy (Zeenite 700P, Analytical Jena) at 25°C. Every experiment was run in triplicate and average values were used in the results. The optimum contact time was examined by repeating the above step with adjusting the pH value at its optimum measuring value and the atomic absorption was measured after different contact times (1 to 24h). The alumina removal efficiency is calculated according to<sup>[14]</sup>.

$$\text{Removal (Adsorption) efficiency \%} = 100 \times (C_0 - C_f) / C_0 \quad (1)$$

where C<sub>0</sub> and C<sub>f</sub> are the initial and final concen-

trations (mg/L) of lead ion solution, respectively.

## RESULTS AND DISCUSSION

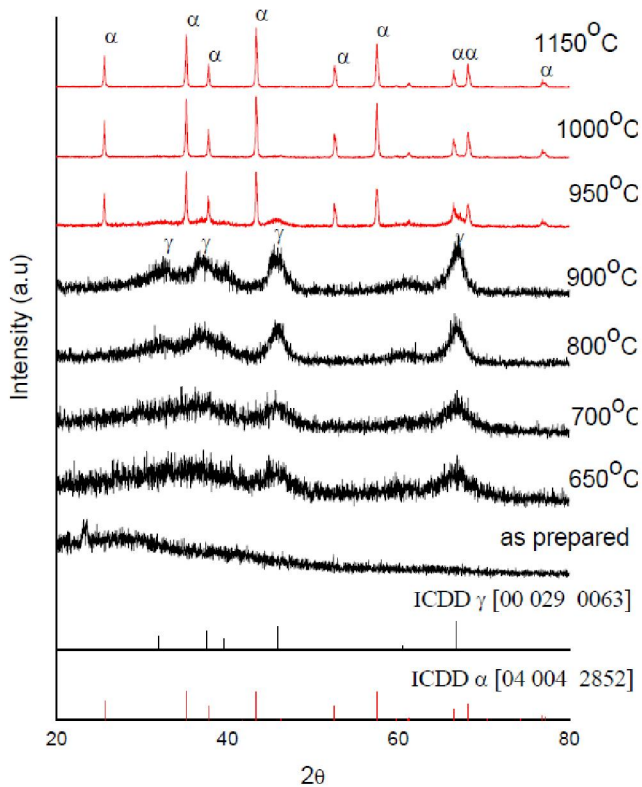
### XRD analysis

Figure (1) illustrates XRD pattern at room temperature for the prepared samples calcined in air at different temperatures combined with [ICDD 00 029 0063] and [ICDD 04 004 2852] of γ-Al<sub>2</sub>O<sub>3</sub> and α-Al<sub>2</sub>O<sub>3</sub> respectively. XRD pattern for the as-prepared sample without any heat treatment shows a diffuse peak indicating amorphous structure of this sample. After annealing the samples in air at 650°C and 700°C, the diffraction peaks can be indexed as the major diffractions of γ-Al<sub>2</sub>O<sub>3</sub> [ICDD 00 029 0063]. The appearance of broaden peaks at 700°C confirm the formation of γ-Al<sub>2</sub>O<sub>3</sub> with very small nanoparticle (2.8nm), based on the Scherrer equation; the crystallite size of a sample is inversely proportional to the full-width at half maximum (FWHM). With reaching the annealing temperature to 900°C a better crystallinity was obtained with completely identifications of [ICDD 00 029 0063]. This implies that, the stability of the single phase formation of γ-Al<sub>2</sub>O<sub>3</sub>, with cubic spinel structure and space group Fd-3m began from 650°C and settled up to 900°C. With increasing the calcination temperature to more than 950°C, the cubic structure is deformed and converted into hexagonal shape and a perfect phase formation of α-Al<sub>2</sub>O<sub>3</sub> with space group R-3C was obtained as matched with the [ICDD 04 004 2852]. Accordingly, these results give single metastable phase of γ-Al<sub>2</sub>O<sub>3</sub> in the temperature range 650°C < T ≤ 900°C and stable single phase of α-Al<sub>2</sub>O<sub>3</sub> from 900°C to above 1150°C (900°C < T > 1150°C). The comparison with the results of Ref.<sup>[13]</sup> confirms that, the two phases of alumina were successfully prepared in the present work at lower annealing temperatures and better crystallinity.

The lattice parameters (a, b, c) of the investigated system have been calculated for the cubic structure (a=b=c) using the relation

$$a = d_{hkl} \sqrt{(h^2 + k^2 + l^2)}, \quad (2)$$

and for the hexagonal structure system were calculated using the relation<sup>[14]</sup>



**Figure 1 :** The XRD patterns of the aluminum oxide nanoparticles annealed in air at different temperatures for 2h with the ICDD cards [00 029 0063] and [04 004 2852]

$$1/d_{hkl}^2 = 4(h^2 + hk + k^2)/3a^2 + l^2 \quad (3)$$

Here  $(h, k, l)$  are the Miller indices and  $d_{hkl}$  is the corresponding d-spaces. Also, the particle size  $D$  has been calculated, from the X-ray data, using the Scherrer's equation<sup>[43, 44]</sup>

$$D = K\lambda/\beta\cos\theta \quad (4)$$

$K$  is the particle shape factor,  $\lambda$  is the target wavelength,  $\beta$  is the full-width at half maximum, and  $\theta$  is the position (angle) of the maximum peak.

The calculated particle size  $D$  and the lattice

parameters for the unit cell are reported in TABLE 1 at different annealing temperatures. It is noted that, the calculated values of the lattice parameters agree adequately with that of the ICDD cards [00 029 0063 and 04 004 2852]. It is known that<sup>[20]</sup> the calculated particle size is defined as the center-to-center distance between two neighbor particles. With increasing the annealing temperature from 650°C to 1150°C, the particle size increases from 2.8nm to 147nm, in other words the center-to-center distance between particles was increased from 2.8nm to 147nm. The condensation and growth of this inter particles distance play a significant role in the physical properties of the samples (porosity, hardness adsorption, and so on).

### Thermal analysis

In order to clarify the thermal stability of the prepared alumina samples the quantitative TGA-DTA analysis was estimated. When the precursor powder was heated in Nitrogen atmosphere three distinct weight losses were observed as shown in Figure [2: a, b]. According to TGA curve, the as synthesized material shows slight mass loss of about -4% from 26°C to 100°C. On the other hand, the major mass loss is observed at 100°C to 249°C. It is of the order -70%. The last mass loss that is about -6% occurs in the temperature range from 249°C to 654°C.

DTA curve shows two main endothermic peaks at about 213°C and 307°C. They are corresponding to the evaporation of the absorbed water and to the evaporation of the constitution water in the aluminum hydroxide  $Al(OH)_3$ . Moreover, some of the other exothermic peaks appear in the temperature range from 370 to 781°C. They are associated with the

**TABLE 1 :** The calculated XRD parameters at different annealing temperature

T (°C)	Particle size (nm)	Structure	Calculated cell parameter			ICDD card cell parameter		
			a (Å)	c (Å)	Volume Å <sup>3</sup>	A (Å)	C (Å)	Volume Å <sup>3</sup>
650	2.4	Cubic	7.9235		497.46			
700	2.8	Cubic	7.9217		497.12	7.9240		497.55
800	3.8	Cubic	7.9207		497.10			
900	3.6	cubic	7.8693		487.30			
950	80	hexagonal	4.7209	13.0126	251.12			
1000	88	hexagonal	4.7601	12.9555	254.23	4.7602	12.9933	254.98
1150	147	hexagonal	4.7472	13.0174	254.05			

## Full Paper

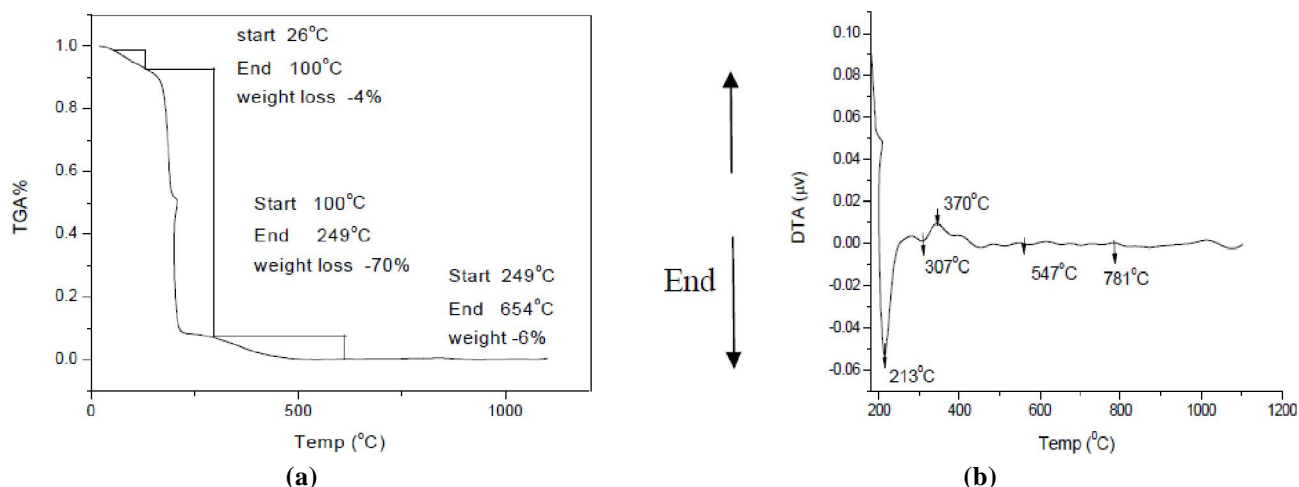


Figure 2 : Thermal analysis of the as prepared alumina (a) TGA and (b) DTA

conversion precursor of.



It is worthwhile noting that, no mass loss occurred above 781°C. This, in turn, indicates that the metastable state  $\gamma\text{-Al}_2\text{O}_3$  is already formed before 781°C. This result agrees with that obtained from XRD analysis. The endothermic peak at 1012°C corresponds to the formation of  $\alpha\text{-Al}_2\text{O}_3$ . Accordingly, it is concluded that, the experimental techniques considered in this work confirmed the formation of metastable of  $\gamma\text{-Al}_2\text{O}_3$  and  $\alpha\text{-Al}_2\text{O}_3$  at lower temperatures than those reported previous work<sup>[18, 20- 22]</sup>.

### FTIR

Figure (3) shows the FTIR spectra for  $\text{Al}_2\text{O}_3$  annealing at different temperatures. The figure displays broad bands around  $3500\text{cm}^{-1}$  and  $1630\text{cm}^{-1}$ . They are assigned to stretching and bending modes of adsorbed water<sup>[4]</sup>. It is well known that<sup>[4]</sup>, the bands in the region of  $400\text{--}1000\text{cm}^{-1}$  are generally associated with the stretching vibration of Al–O bonds. The identification of the obtained bands for the sample annealed at  $700^\circ\text{C}$  referred to the formation of  $\gamma$  alumina. The appearance of very small Al–O stretching modes of  $[\text{AlO}_6]$  at  $767$ ,  $624$ , and  $579\text{cm}^{-1}$ , in addition to the two bands at  $1434\text{cm}^{-1}$  and  $1512\text{cm}^{-1}$  confirmed the formation of  $\gamma$  alumina. The intensity of the bands in the region  $400\text{--}1000\text{cm}^{-1}$  increases with increasing the annealing temperature which clarifies a better crystallinity of  $\gamma$  alumina formed at  $900^\circ\text{C}$ . It is noted that the phase transformation was obtained when the calcination tempera-

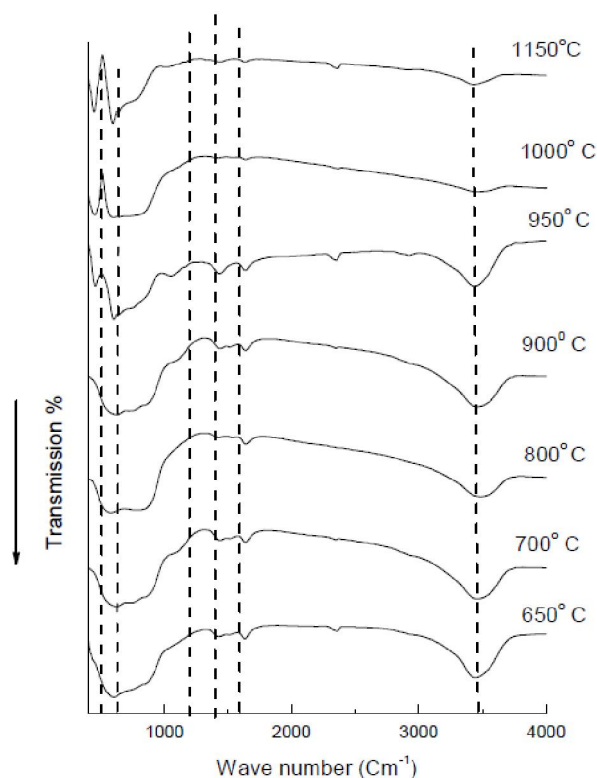
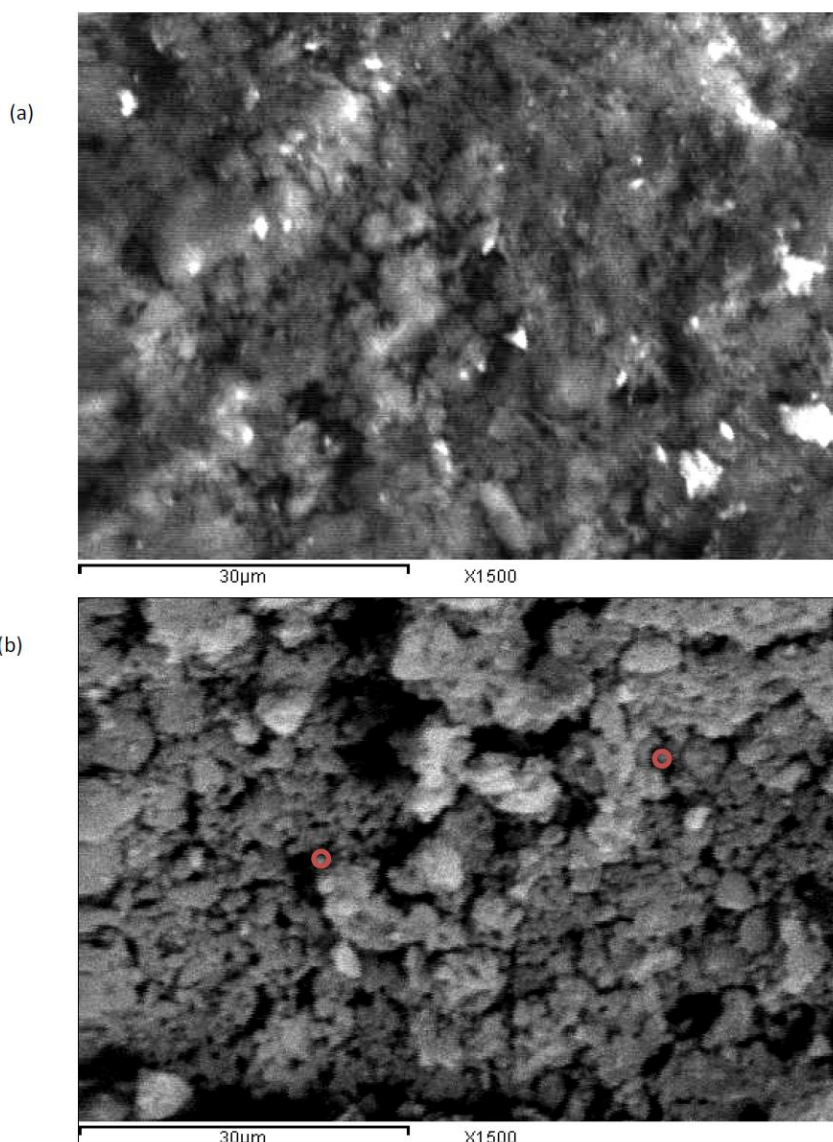


Figure 3 : FTIR spectra of the alumina samples annealed at  $650^\circ\text{C}$ ,  $700^\circ\text{C}$ ,  $800^\circ\text{C}$ ,  $900^\circ\text{C}$ ,  $950^\circ\text{C}$ ,  $1000^\circ\text{C}$  and  $1150^\circ\text{C}$

ture become greater than  $900^\circ\text{C}$ , where the bands  $576$  and  $763\text{cm}^{-1}$  disappeared and new bands were formed at about  $450$ ,  $591$ ,  $650$  and  $1113\text{cm}^{-1}$ . These results are consistent with those reported in Refs.<sup>[17, 21, 23, 45- 46]</sup>.

### SEM

The size and morphology of the particles were further characterized by the scanning electron mi-



**Figure 4 (a, b) : SEM micrographs of (a)  $\gamma$ -alumina annealed at 900°C and (b)  $\alpha$ -alumina annealed at 1000°C**

croscopie (SEM). Figure (4: a, b) illustrates the (SEM) micrograph of the prepared alumina annealed at 900°C and 1000°C. Very fine particles aggregated in large grains in platelets form with irregular geometrical shape appeared in the micrograph of the  $\gamma$ -alumina sample that is beside the presence of very small pores. The  $\alpha$ -alumina micrograph is characterized by better crystallinity of small spherical particles slightly accumulated and surrounded by some large pores. These micrographs promised that, the annealing temperature increases the particle size and improves the crystallinity of the prepared samples.

Figure (5: a, b) shows the EDX quantitative analysis of  $\gamma$ - $\text{Al}_2\text{O}_3$  and  $\alpha$ - $\text{Al}_2\text{O}_3$  annealed at 900°C and 1000°C respectively. The data assured the pure

preparation of the samples. The obtained weight percentage of each of Al and O were in comparable values with the stoichiometric ratio of  $\text{Al}_2\text{O}_3$  with a slight increase of the oxygen ratio that is due to the performance of annealing in air.

### BET analysis

The prepared alumina was characterized by  $\text{N}_2$ -adsorption / desorption measurements (BET Analysis). The surface area, average pore size and pore volume analysis of  $\alpha$ - $\text{Al}_2\text{O}_3$  and  $\gamma$ - $\text{Al}_2\text{O}_3$  were determined and provided in TABLE (2). The data clarified that,  $\gamma$ - $\text{Al}_2\text{O}_3$  characterized by large surface area and large pore volume. Accordingly, it is recommended that  $\gamma$ - $\text{Al}_2\text{O}_3$  can be used in the purification

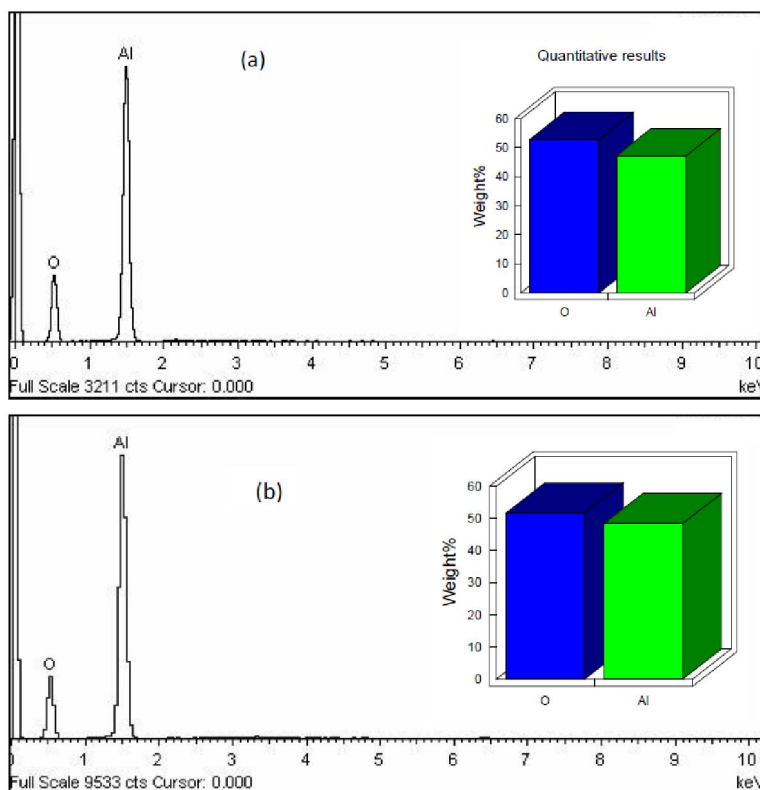


Figure 5(a, b) : EDX analysis of (a)  $\gamma$ -alumina annealed at 900°C and (b)  $\alpha$ -alumina annealed at 1000°C

TABLE 2 : The calculated BET parameters: Surface area (S), Pore volume ( $P_v$ ) and Pore diameter ( $P_d$ ) of each of  $\gamma$ - $Al_2O_3$  and  $\alpha$ - $Al_2O_3$

Sample	S ( $m^2/g$ )	$P_v$ ( $cm^3/g$ )	$P_d$ (nm)
$\gamma$ - $Al_2O_3$	136	0.06579	0.193
$\alpha$ - $Al_2O_3$	19.29	0.00921	0.191

and desalination of water. On the other hand, the data indicated that  $\alpha$ - $Al_2O_3$  is preferably employed to support a desalination membrane.

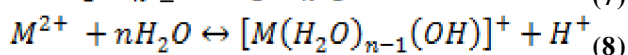
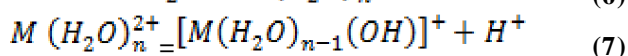
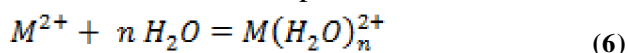
### AFM

Atomic force microscope (AFM) is a powerful tool for the determination of topography and the roughness in even nano-scale. Figure (6: a, b) represents AFM (non-contact mode) 3D topographic images of  $\gamma$ - $Al_2O_3$  annealed at 900°C and  $\alpha$ - $Al_2O_3$  annealed at 1000°C, while the plane image of these two alumina phases is illustrated in Figure (7: a, b). It is shown that, the height difference for  $\alpha$ - $Al_2O_3$  is 279.45nm while that for  $\gamma$ - $Al_2O_3$  is 303.31nm, this means that; Gama alumina characterized by higher roughness surface than Alfa alumina. This is considered as a reasonable guide for the application of  $\gamma$ - $Al_2O_3$  as catalyst support and in adsorption of toxic metals because of its roughness and large surface

area, while,  $\alpha$ - $Al_2O_3$  can be used as a support in fabrication of water desalination membrane.

### Adsorption studies

Most of atoms are unsaturated on the nanoparticles surface and can easily bind with other atoms. Nanoparticles are characterized by high adsorption capacity, besides, rapid adsorption process<sup>[47]</sup>. The metal ions in the aqueous solution may undergo solvation and hydrolysis. The process involved for metal adsorption is as follows<sup>[14]</sup>.



The colloidal stability of suspensions of alumina particles has been investigated by measuring zeta potential. Zeta potential ( $\zeta$ ) was determined as a function of pH. When particles are dispersed in an

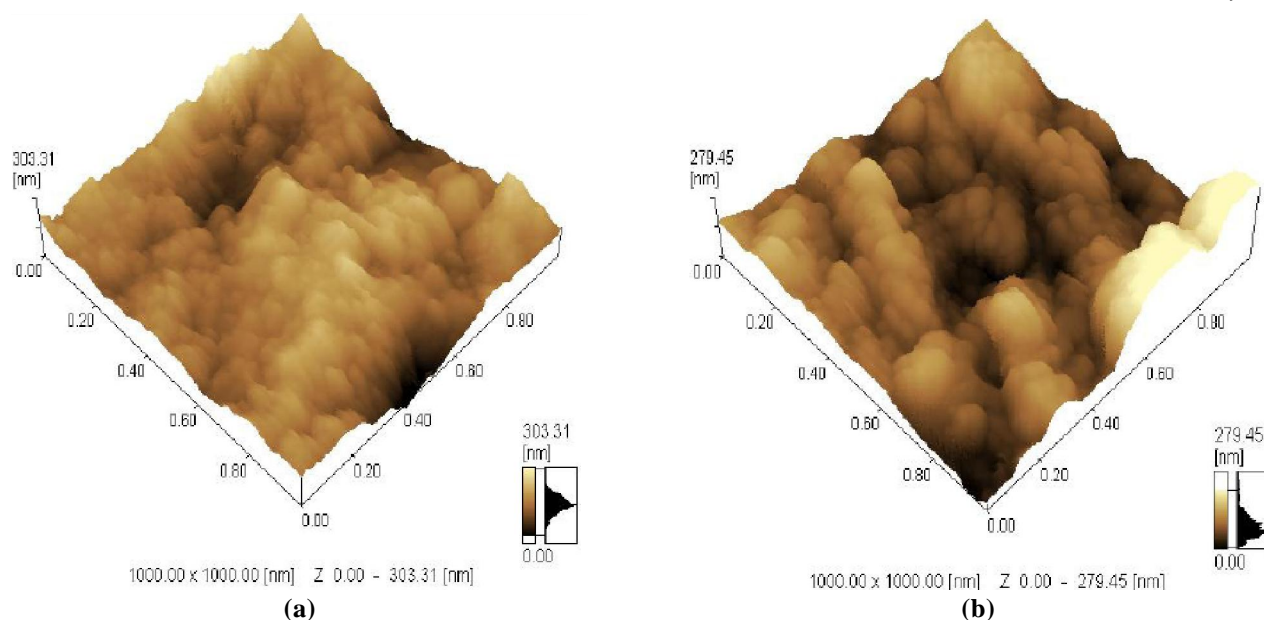


Figure 6(a, b) : 3D AFM image of (a)  $\gamma$ -Al<sub>2</sub>O<sub>3</sub> annealed at 900°C and (b)  $\alpha$ -Al<sub>2</sub>O<sub>3</sub> annealed at 1000°C

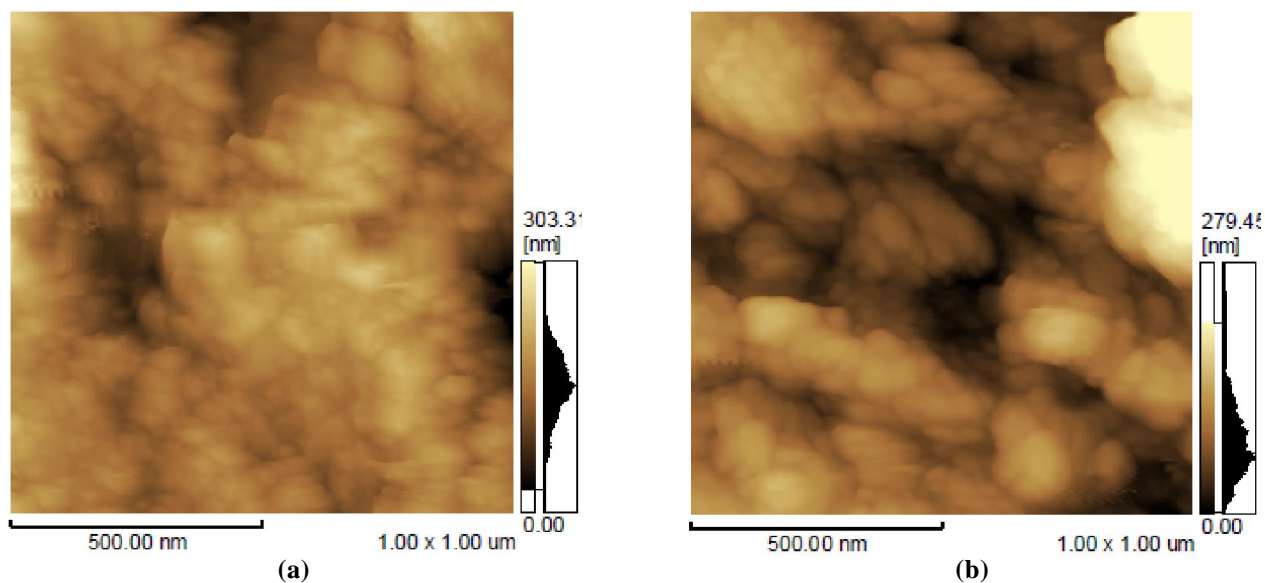


Figure 7 : AFM plane image of (a)  $\gamma$ -Al<sub>2</sub>O<sub>3</sub> annealed at 900°C and (b)  $\alpha$ -Al<sub>2</sub>O<sub>3</sub> annealed at 1000°C

aqueous medium, the surface charges on the particles are bound to influence the state of dispersion or aggregation by the particles. A well dispersed substance can be obtained with high surface charge density to generate strong repulsive force. The surface chemical properties of the powder were determined by the H<sup>+</sup> and OH<sup>-</sup> ions adsorb on the particle surface<sup>[48,49]</sup>. If all suspended particles have large negative or positive zeta potential then they tend to repel each other and there is no tendency to flocculate. If the particles have low zeta potential, then there is no force preventing the particles coming together and

flocculating. Particles with zeta potential more positive than +30 mV or more negative than -30 mV are normally considered stable<sup>[14]</sup>. Figure (8: a, b) shows the effect of pH value on zeta potential of  $\gamma$  and  $\alpha$ -alumina. The isoelectric point (iep) is the point at which the surface concentration of H<sup>+</sup> and OH<sup>-</sup> are equal. The (iep) of  $\gamma$  and  $\alpha$ - alumina powder were found at pH equals 4.3 and 6.5 respectively. The surface charge is negative at pH greater than (iep) and positive at pH less than (iep). From Figure (8: a, b), the particle is stable at pH 9 because  $\zeta$  reached to its largest value and it was larger than -30 mV.

## Full Paper

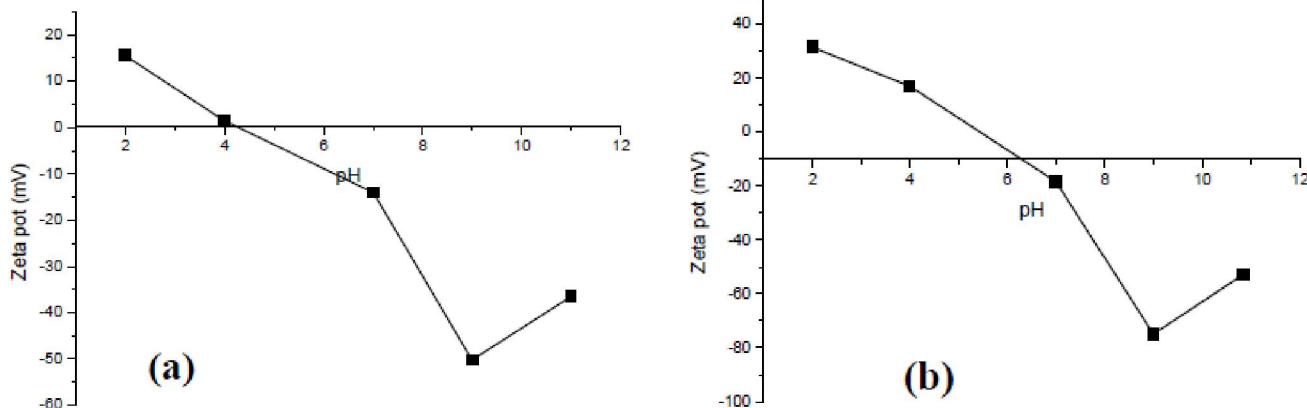


Figure 8(a, b) : Zeta potential in water as function of pH of (a)  $\gamma$ - $\text{Al}_2\text{O}_3$  annealed at  $900^\circ\text{C}$  and (b)  $\alpha$ - $\text{Al}_2\text{O}_3$  annealed at  $1000^\circ\text{C}$

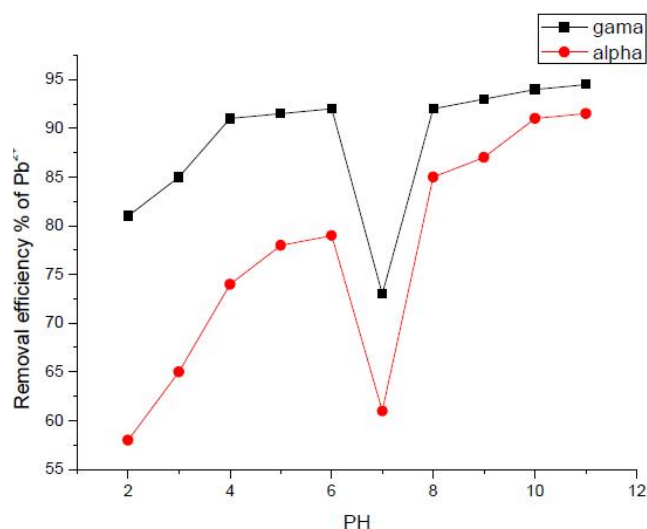


Figure 9 : The dependence of the removal percent of  $\text{Pb}^{2+}$  using  $\alpha$ - $\text{Al}_2\text{O}_3$  and  $\gamma$ - $\text{Al}_2\text{O}_3$  on the pH values. Conditions: sorbent concentration  $2\text{mg/L}$ , temperature  $293\text{K}$  and contact time  $1\text{h}$

Similar trend was for the dependence of  $\zeta$  potential on the pH values for both of  $\gamma$  and  $\alpha$ - $\text{Al}_2\text{O}_3$  with slightly increase in its value of  $\alpha$ - $\text{Al}_2\text{O}_3$  than that of  $\gamma$ - $\text{Al}_2\text{O}_3$  which indicates that the  $\alpha$ - $\text{Al}_2\text{O}_3$  is more stable than  $\gamma$ - $\text{Al}_2\text{O}_3$ .

The pH value of the solution has a significant impact on the uptake of heavy metals, since it determines the surface charge of the adsorbent and the degree of ionization<sup>[14]</sup>. In order to establish the effect of pH on the adsorption of  $\text{Pb}^{2+}$ , the atomic absorption measurements were carried out for lead nitrate solution adjusted at pH ranged (2 to 11) as discussed above in the experimental part. The removal efficiency was calculated according to Eq. (1). It is well known that<sup>[47]</sup>, at higher pH values, the  $\text{OH}^-$  on

the surface of nanostructure alumina provides the ability of binding cations. The decrease of pH passing by the neutralization of surface charge causes the  $\text{OH}^-$  to be displaced from the surface. A continuous decrease of pH creates a surface of nanoparticles alumina which carries +ve charges and this is a suitable condition to adsorb anions<sup>[47]</sup>. Although, the data in Figure (9) shows nearly equal removal percent at pH 6 and 9, but the favorable experimental work is considered at pH 6. This is due to as pH of the solution increased  $\sim 7$ , Pb started to precipitate out from the solution and the removal percentage calculation is increased as the resultant of the combination of both adsorption and precipitation effects<sup>[47]</sup>. Accordingly, pH 6 is the optimum value for  $\text{Pb}^{2+}$  adsorption. A closer look to Figure (9) illustrates higher removal percent of  $\gamma$ - $\text{Al}_2\text{O}_3$  than that of  $\alpha$ - $\text{Al}_2\text{O}_3$ , this is back to  $\gamma$ - $\text{Al}_2\text{O}_3$  characterized by smaller particle size as clarified from TABLE 1, higher surface area and higher pore volume as determined from BET data and reported in TABLE 2.

Figure (10. a) illustrated a comparison between the contact time effect on the removal efficiency of  $\gamma$  alumina for  $\text{Pb}^{2+}$  ions at pH 6 and 9. It is clear that, the adsorption efficiency increased with contact time and its value for pH 9 is higher than that of pH 6. As discussed above, this reveals that the removal of  $\text{Pb}^{2+}$  at pH 6 is only due to the alumina adsorption, while at pH 9 there are two factors affecting on the removal mechanism, the adsorption effect and the chemical precipitation process<sup>[14]</sup>. Figure (10: b) shows the effect of contact time on the removal of

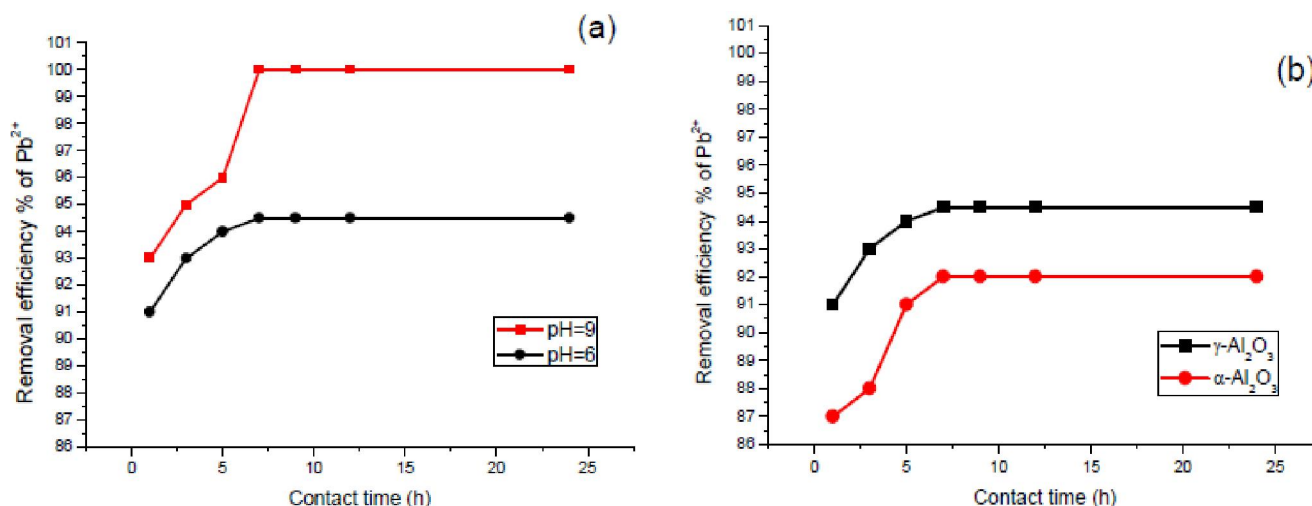


**Figure 10(a, b) :** The conditions: sorbent concentration 2mg/L and temperature 293K; (a) Effect of contact time on the removal percentage of Pb<sup>2+</sup> at pH 6 and pH 9 using  $\gamma$ -Al<sub>2</sub>O<sub>3</sub>; (b) Effect of contact time on the removal percentage of Pb<sup>2+</sup> at pH 6 using each of  $\gamma$ -Al<sub>2</sub>O<sub>3</sub> and  $\alpha$ -Al<sub>2</sub>O<sub>3</sub>.

Pb<sup>2+</sup> ions from water at pH 6 using the two alumina phases. It is noted that, the removal efficiency percentage, using  $\gamma$  alumina, reached to about 91% after 1h

and up to 94.5% after 7h. This can be interpreted as follows, the removal process occurs in two steps, at the beginning alumina has rapid uptake and then followed by slower uptake. The rapid uptake is associated with the external surface adsorption, and when all the active sites are occupied, the equilibrium is reached and the rate of alumina uptake decreased. The results of this work clarified that, the efficiency of the prepared  $\gamma$  and  $\alpha$  alumina nanoparticle to remove Pb<sup>2+</sup> from water after 7h is reached to ( $\approx$ 94.5% and 92%) respectively. These results attained economic fruitful outcomes where low cost was required for preparing nano  $\gamma$  alumina phase with highly removal efficiency.

## CONCLUSION

$\gamma$ -Al<sub>2</sub>O<sub>3</sub> and  $\alpha$ -Al<sub>2</sub>O<sub>3</sub> phases have been synthesized at low annealing temperature 650°C and 950°C respectively via reverse microemulsion route using Triton (X-100) as surfactant and Butanol as co-surfactant. The removal efficiency of lead 2mg/L from water increased with contact time, its values at pH 6 after 7h reached to ( $\approx$ 94.5%) and (92%) using 0.1g of nanoparticles powder of  $\gamma$  and  $\alpha$  alumina respectively. These results backed to the smaller particle

size, highly roughness, larger surface area and porosity volume of  $\gamma$ -Al<sub>2</sub>O<sub>3</sub> than that of  $\alpha$ -Al<sub>2</sub>O<sub>3</sub> phases. Accordingly,  $\gamma$ -Al<sub>2</sub>O<sub>3</sub> is recommended to use in purification of water, while,  $\alpha$ -Al<sub>2</sub>O<sub>3</sub> is preferably employed to support the desalination membrane.

## REFERENCES

- [1] J.B.Brower, R.L.Rayan, M.Pazirandeh, Environ.Sci.Technol., **31**, 2910–2914 (1997).
- [2] X.Zhang, S.Lin, X.Q.Lu, Z.Chen; Chemical Engineering Journal, **163**, 243-248 (2010).
- [3] M.A.Ahmed, S.M.Ali, S.I.El-Dek, A.Galal; Materials Science and Engineering B **168**, 744–751 (2013).
- [4] L.Jarup, M.Berglund, C.G.Elinder, G.Norberg, M.Vahter; Scand.J.Enviro.n.Health, **24**(1), 1–51 (1998).
- [5] L.Yan-Ui, Z.Yanqiu, Z.Yimin, W.Dehai, L.Zhaokun; Diamond and Related Materials, **15**, 90–94 (2006).
- [6] Z.Elouear, J.Bouزيد, N.Boujelben, M.Feki, F.Jamoussi, A.Montiel; Journal of Hazardous Materials, **156**, 412–420 (2008).
- [7] J.T.Mayo; Science Technology and Advanced Materials, **8**, 71–75 (2007).
- [8] R.Leyva-Ramos, J.R.Rangel-Mendez, J.Mendoza-Barron, L.Fuentes-Rubio, R.M.Guerrero-Coronado; Water Science and Technology, **35**, 205–211 (1997).
- [9] E.Korngold, S.Belfer, C.Urtizberea; Desalination, **104**, 197–201 (1996).
- [10] C.N.Mulligan, R.N.Yong, B.F.Gibbs; Engineering Geology, **60**, 193–207 (2001).
- [11] S.M.C.Ritchie, D.Bhattacharyya; Journal of Hazardous Materials, **111**, 1–10 (2004).

## Full Paper

- ardous Materials, **92**, 21–32 (2002).
- [12] V.M.Boddu, K.Abburi, J.L.Talbott; Environmental Science and Technology, **37**, 4449–4456 (2003).
- [13] G.Crini; Progress in Polymer Science, **30**, 38–70 (2005).
- [14] T.K.Naiya, A.K.Bhattacharya, S.K.Das, J.of Colloid and Interface Science, **333**, 14–26 (2009).
- [15] Y.Xi, M.Mallavarapu, R.Naidu; Materials Research Bulletin, **45**, 1361–1367 (2010).
- [16] V.D.Zhuravlev, V.G.Bamburov, A.R.Beketov, L.A.Pereleyaeva, I.V.Baklanova, O.V.Sivtsova, V.G.Vasil'ev, E.V.Vladimirova, V.G.Shevchenko, I.G.Grigorov; Ceramics International **39**, 1379–1384 (2013).
- [17] L.Zhu, S.Pu, K.Liu, T.Zhu, F.Lu, J.Li; Materials Letters, **83**, 73–75 (2012).
- [18] K.Huang, L.Yin, S.Liu, C.LI; T.Nonferrous Met.Soc.China, **17**, 633–637 (2007).
- [19] S.Xinghua, C.Shuanfa, Z.Zhenjun; Applied Surface Science, **258**, 5712–5715 (2012).
- [20] A.K.Patra, D.Arghya, B.Asim; Journal of Hazardous Materials, **201–202**, 170–177 (2012).
- [21] T.Zaki, K.I.Kabel, H.Hassan; Ceramics International, **38**, 2021–2026 (2012).
- [22] Q.Liu, A.Q.Wang, X.H.Wang, W.D.Guo, T.Zhang; Micropor Mesopor Mater., **111**, 323–333 (2008).
- [23] Y.Adraider, S.N.B.Hodgson, M.C.Sharp, Z.Y.Zhang, F.Nabhani, A.Al-Waidh; J.of the European Ceramic Society, **32**, 4229–4240 (2012).
- [24] J.M.Andersson; Linköping University, SE-581 83 Linköping, Sweden, (2005).
- [25] W.Q.Jiao, M.B.Yue, Y.M.Wang, M-Y.He.Microporous Mesoporous Mater, **147**, 167–77 (2012).
- [26] Z.Zhang, R.W.Hicks, T.R.Pauly, T.J.Pinnavaia; J.Am.Chem.Soc., **124**, 1592 (2002).
- [27] S.Wang, X.Li, S.Wang, Y.Li, Y.Zhai; Mater Lett, **62**, 3552 (2008).
- [28] J.Cejka; Appl.Catal.A: Gen., **254**, 327–338 (2003).
- [29] M.Trueba, S.P.TrasattiEur.J.Inorg.Chem., **17**, 3393–3403 (2005).
- [30] M.H.Yuan, C.Y.Chang, J.L.Shie, C.C.Chang, J.H.Chen, W.T.Tsai; J.Hazard.Mater, **175**, 809–815 (2010).
- [31] K.Shimizu, M.Nishimura, A.Satsuma; Chem Cat Chem., **1**, 497–503 (2009).
- [32] M.Paul, N.Pal, A.Bhaumik; Eur.J.Inorg.Chem., **32**, 5129–5134 (2010).
- [33] X.S.Fang, C.H.Ye, X.X.Xu, T.Xie, Y.C.Wu, L.D.Zhang; J.Phys.: Condensed.Matter, **16**, 4157–4163 (2004).
- [34] J.Robertson, B.Falabretti; J.Appl.Phys., **100**, 014111 (2006).
- [35] G.Lee, C.Chen, S.T.Yang, W.S.Ahn; Microporous Mesoporous Mater., **127**, 152–156 (2010).
- [36] X.Y.Zhang, J.Zhao, A.V.Whitney, J.W.Elam, R.P.Van Duyn; J.Am.Chem.Soc., **128**, 10304–10309 (2006).
- [37] V.Jarayaman, T.Guanasekaran, G.Periaswami; Mater.Lett., **30**, 157 (1997).
- [38] X.R.Huang, G.L.Meng, Z.T.Huang, J.M.Geng; J.Membr.Sci., **133**, 145 (1997).
- [39] A.F.M.Leenaars, A.J.Burggraaf; J.Colloid Interface Sci., **105**, 27 (1985).
- [40] C.R.Xia, F.Wu, Z.J.Meng, F.Q.Li, D.K.Peng, G.Y.Meng; J.Membr.Sci., **116**, 9 (1996).
- [41] A.Mahapatra, B.G.Mishra, G.Hota; Ceram.Int., **37**, 2329–2333 (2011).
- [42] M.Bontonnet, J.Kizlinc, P.S.Gihert; J.Colloids and Surfaces, **5**, 209–225 (1982).
- [43] B.D.Cullity; “Elements of X-ray Diffraction”, Copyright, Addition-Wesley Publishing Company, Inc., (1956).
- [44] F.Mirjalili, M.Hasmaliza, L.Chuah Abdullah; Ceramics International, **36**, 1253–1257 (2010).
- [45] Y.X.Pang; J.European Ceramic Society, **32**, 4229–4240 (2012).
- [46] J.Li, X.Wang, L.Wang, Y.Hao, Y.Huang, Y.Zhang, X.Sun, X.Liu; J.Membr.Sci., **275**, 6–11 (2006).
- [47] A.Rahmani, H.Zavvar Mousavi; M.Fazli Desalination, **253**, 94–100 (2010).
- [48] B.P.Singh, R.Menchavez, C.Takai, M.Fuji, M.Takahashi; J.of Colloid and Interface Sci., **291**, 181–186 (2005).
- [49] Leader on colloidal dynamic “The Zeta Potential”, www.colloidal-dynamics.com (1999).